Appl Magn Reson (2010) 37:851–864
DOI 10.1007/s00723-009-0091-6

Applied
Magnetic Resonance

A High-Conversion-Factor, Double-Resonance Structure for High-Field Dynamic Nuclear Polarization

G. Annino · J. A. Villanueva-Garibay · P. J. M. van Bentum · A. A. K. Klaassen · A. P. M. Kentgens

Received: 19 May 2009 / Revised: 25 June 2009 / Published online: 14 November 2009

Abstract This contribution presents a novel design of a double-resonance structure for high-field dynamic nuclear polarization operating at 95 GHz and 144 MHz, in which a miniaturized radiofrequency coil is integrated within a single-mode nonradiative dielectric resonator. After a detailed discussion of the design principles, the conversion factors of this system are determined by means of microwave and radiofrequency measurements. The obtained results, 1.68 mT/W$^{1/2}$ for the microwave conversion factor and 0.8 mT/W$^{1/2}$ for the radiofrequency conversion factor, represent the state-of-the-art among the double-resonance structures. Simultaneous electron paramagnetic resonance and liquid-state ^{1}H nuclear magnetic resonance experiments are performed on samples of nitroxide radical 2,2,6,6-tetramethylpiperidine-1-oxyl dissolved in a mixture of water and dioxane. A maximum dynamic nuclear polarization enhancement of about −16 is obtained at a microwave power of 70 mW with a radical concentration of 10 mM in nanoliter-sized sample volumes. These results are discussed in view of further improvements and applications of the proposed double-resonance structure.

1 Introduction

Dynamic nuclear polarization (DNP) is a double-resonance technique that may help to overcome sensitivity problems in nuclear magnetic resonance (NMR) measurements. This low sensitivity is ultimately due to the low magnetic energy of the nuclear spins with respect to the thermal energy at room temperature, leading to a

G. Annino (✉)
Istituto per i Processi Chimico-Fisici, CNR, via G. Moruzzi 1, 56124 Pisa, Italy
e-mail: geannino@ipcf.cnr.it

J. A. Villanueva-Garibay · P. J. M. van Bentum · A. A. K. Klaassen · A. P. M. Kentgens
Institute for Molecules and Materials, Radboud University Nijmegen,
Toernooiveld 1, 6525 ED Nijmegen, The Netherlands

very modest polarization of the nuclear spins. One of the main problems encountered in the development of instrumentation for high-field DNP concerns efficient equipment in both the microwave (mw) and radiofrequency (rf) response. This would greatly reduce the microwave power necessary to obtain a given sensitivity enhancement.

The aim of DNP is to transfer the much larger electronic polarization of unpaired electrons to the abundant nuclei in the sample. This possibility was first pointed out by Overhauser, who predicted the DNP mechanism in metals [1], and later proved by Carver and Slichter [2]. The maximum theoretical polarization enhancement for protons is of the order of the gyromagnetic ratios $\gamma_e/\gamma_n = 660$. After the seminal work of Overhauser, other DNP mechanisms have been identified, such as the solid effect [3], the cross effect [4–8], and the thermal mixing [9]. A comprehensive review of these mechanisms has recently been published by Griffin and coworkers [10].

Experimental confirmation of the predicted DNP enhancements, both in the liquid and solid states, is well established [11–16]. Polarization transfer at cryogenic temperatures has the additional advantage of the more favorable low-temperature Boltzmann factors. Using a rapid dissolution of the prepolarized sample one can achieve impressive signal enhancements of four orders of magnitude [17]. Commercial vendors have made the dissolution method available for mainstream NMR (Oxford Instruments Biotools, UK). Instrumentation for solid-state DNP, combined with in situ magic-angle spinning (MAS) NMR spectroscopy, has recently become available from the Bruker company. A comprehensive survey of the state-of-the-art in DNP is provided by a recent special issue of Applied Magnetic Resonance [18].

Despite the impressive progress in the field of DNP methodology and instrumentation, there are various issues that require further study and optimization. For instance, in the dissolution method, the low-temperature polarization is a slow process (which often requires several hours) and the NMR experiment is necessarily limited to a single or a few scans within the T_1 time frame of the nuclei. Proton NMR is generally not feasible and multidimensional NMR is only possible in the context of gradient-encoded single-scan methodology [19–22]. Solid-state MAS-DNP requires ultra-low temperature MAS probes. In general, it is not possible to work with high-Q resonators, especially at the high frequencies commensurate with the modern high-field NMR spectrometers. For this reason, millimeter-wave sources are developed with very high output powers. The most common sources are gyrotrons operating at 10 W or higher power levels [10, 23–27]. These sources need their own high-field cryomagnets, which further complicate the experimental configuration. Overhauser DNP in the liquid state is hampered by the fact that the coupling parameters are reduced at high frequencies, and the effective enhancement is reduced as the magnetic field levels increase above a few Tesla. In addition, the stronger dielectric absorption in aqueous solutions lead to substantial mw heating at the power levels needed to saturate the electronic transitions.

For all polarization mechanisms that proved effective in DNP studies, the enhancement of the NMR signal generated by the electron paramagnetic resonance (EPR) transitions increases with the intensity of the mw magnetic field, until these transitions are fully saturated [28]. In this context, the mw resonance structure

becomes the key element of a DNP spectrometer. For a given quality factor Q of the device, the intensity of the oscillatory magnetic field B in the resonator is related to the available power P through the expression $B^2 \propto Q{\cdot}P$ [29]. Moreover, the field distribution inside a resonator can be in general carefully controlled, allowing a spatial separation of the magnetic field nodes from the electric field nodes, which is necessary to both limit the dielectric absorption and avoid an excessive heating of the sample.

For efficient NMR excitation and detection a microcoil configuration with an optimal coupling and filling factor is required [30]. This microcoil needs to be placed inside the mw resonator with minimal impact on the mw mode structure and conversion factor, and matched to a resonant circuit.

At low magnetic fields, the construction of such a double-resonance structure is simplified by the relatively large wavelength of the mw radiation. At high magnetic fields, typically above 3 T, the wavelength of the radiation ranges from a few mm down to about 0.5 mm for the highest-frequency NMR spectrometers that are commercially available. The first mw resonators including rf coils were based on oversized cavities, whose dimensions exceed the resonant wavelength [31–33]. However, the efficiency in converting the available power in mw magnetic field is relatively modest. Better performances are obtained by employing a cylindrical single-mode cavity with a slotted surface, which allows a partial penetration of the rf field generated by a coil placed outside the cavity [34, 35]. However, in this configuration the rf conversion efficiency on the sample is limited by the shielding of the mw cavity wall. This problem has been overcome by using a single-mode TE_{011} cylindrical cavity with a helical surface acting as a rf coil [36–39]. At high frequencies, this design was first employed successfully at 140 GHz [28], and then extended to 260 GHz [40]. Its main limit is the low quality factor of the mw resonator, which is seriously deteriorated by the cut in the cavity wall.

In this contribution, we propose an alternative approach to the design of the double-resonance structure. The main goal is to construct a convenient mw resonant system with an optimal conversion factor and minimized dielectric heating, with in situ NMR options allowing an efficient monitoring of the DNP process and optimization of the polarization transfer parameters.

At frequencies in the millimeter-wave regime, the highest-conversion-factor resonators are single-mode structures, in which the sample volumes are typically in the nanoliter range. Standard electron-nuclear double resonance (ENDOR) configurations use a sensitive EPR detection and, as a compromise imposed by practical reasons, a very low-efficiency NMR coil placed outside the mw resonator, which is used for excitation only. Consequently, for in situ NMR monitoring of DNP at millimeter wavelengths the typical ENDOR configuration is not desirable. Here we describe an alternative in which the NMR coil is incorporated directly inside the mw resonator. The developed system represents a DNP test platform for liquid-state Overhauser DNP operating at W-band frequencies.

The proposed double-resonance structure, designed to operate at 95 GHz and 144 MHz, is based on a mw nonradiative (NR) dielectric resonator. The NR resonators are open single-mode structures capable of state-of-the-art performance at millimeter wavelengths [41, 42]. Further advantages of these resonators are the simple modular structure and the inherently open configuration, which simplifies the

coupling to the mw source and the access to the active region of the device. The rf coil is a simple U-shaped element integrated within the NR resonator. The coil is part of a $\lambda/4$ resonant circuit tuned and matched to the proton NMR frequency.

The power-to-field conversion efficiencies of the proposed double-resonance structure have been assessed from the mw resonance curves and from pulsed NMR measurements. The overall behavior of the resonator has been investigated by room-temperature DNP measurements on aqueous solutions of the 2,2,6,6-tetramethylpiperidine-1-oxyl (TEMPO) nitroxide radical. The design principles of the double-resonance structure are introduced in Sect. 2, while its electromagnetic characterization is described in Sect. 3. The results of the EPR and DNP measurements are presented and discussed in Sect. 4. Some conclusive remarks are given in the last part of this contribution.

2 Design

Different NR resonators have been developed in the context of high-field EPR studies [43–46]. The basic design consists of a central resonant region enclosed between two relatively thick metal plates placed at a distance less than half the wavelength. When the overall structure has rotational invariance, it supports transverse electric (TE) modes that cannot propagate in the planar directions, hence the term 'nonradiative'. The resonance volume can be formed by drilling symmetric holes through the metal plates. If the diameter of these holes is less than the cutoff wavelength for a circular metal waveguide, then the radiation is also confined in the axial direction. In particular, the enclosed volume supports a resonant mode that is very similar to the TE_{011} mode of a conventional cylindrical resonator [41]. The main difference is that the coupling to an external waveguide can be along any planar direction and can be determined by the distance of the excitation system from the axis of the resonator. As for the conventional cavity, the conversion factor of a NR resonator can be increased by inserting a dielectric region in the structure. In this way, unprecedented conversion factors can be obtained [45, 47].

The basic structure of the resonator employed in the present work is shown in Fig. 1a. The mw part is composed by a dielectric tube inserted in two metal plates, in analogy to the design of Ref. [45]. In such a structure, two conditions must be fulfilled for a confined TE_{011} mode, namely $l < \frac{\lambda_0}{2}$ and $r < \frac{3.8317\lambda_0}{2\pi\sqrt{\varepsilon}}$, where λ_0 is the resonance wavelength, l is the distance between the metal plates, r is the radius of the dielectric tube (assumed equal to that of the holes in the metal plates), and ε is its dielectric permittivity [45]. The first equation imposes the non-radiativity along the parallel plates, whereas the second equation imposes the non-radiativity along the axial holes, which represent now circular metal waveguides filled with a dielectric rod (for the sake of simplicity, the dielectric tube is assumed to be a rod). The active volume of the resonator is given by the intersection region between the metal plates and the dielectric tube.

The excitation of the resonator can be obtained by means of a single-mode rectangular waveguide, ending close to its active region, as shown in Fig. 1a. The incoming wave must be polarized parallel to the plates, in order to avoid any

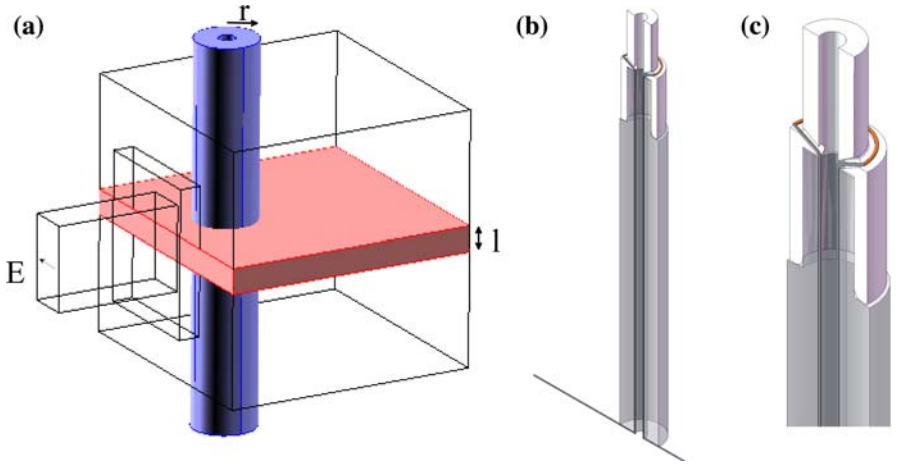

Fig. 1 **a** Schematic drawing of the NR resonator and of its relevant dimensions (see text below). The *light gray* region represents the empty space between the metallic plates, the *dark gray* region is the dielectric tube. The excitation waveguide is shown as well, together with the polarization of the electric field of the incoming radiation. The hollow plunger, allowing the frequency tuning, is not shown for the sake of clarity. **b** Cross-section view of the dielectric tube (*gray region*) with the rf coil and the Teflon cap. **c** Detail of the Teflon cap and the rf wire

leakage of radiation. The control on the coupling level can be obtained by displacing the excitation waveguide with respect to the resonator [43].

In comparison to its basic version shown in Fig. 1a, the actual resonator includes a hollow plunger that enables the mechanical tuning of the resonance frequency. The dielectric part of the resonator consists of a high-purity, ultra-low OH^- content Suprasil® fused quartz tube (Polymicro Technologies, AZ, USA), having an outer diameter of 1.60 ± 0.01 mm and an inner diameter of 0.40 ± 0.01 mm. The dielectric tube is inserted inside two semi-cylindrical copper parts kept at a distance of 1.1 mm, whose planar surfaces are optically polished. One plate is equipped by a hollow plunger with a nominal inner diameter of 1.60 mm. The outer diameter of the plunger is 2.6 mm. The hole in the plate accommodating the plunger has a nominal diameter of 2.60 mm, whereas the hole in the other plate has a nominal diameter of 1.60 mm. The overall diameter of the assembled resonating structure is 11 mm. The head of the plunger is threaded according to the $M3 \times 0.35$ mm mechanical standard. A ring with an external diameter of 16 mm and an internal diameter of 11 mm joins the NR resonator with a WR-08 waveguide. Figure 2a shows an assembled view of the NR resonator including the dielectric tube, whereas Fig. 2b shows the assembled resonator with the connection ring and the excitation waveguide.

In the configuration investigated, the distance between the dielectric tube and the end of the excitation waveguide, which defines the maximum coupling level, was fixed to 0.9 mm. This value led to overcoupled conditions for the empty resonator and an almost critically coupled condition for the different investigated samples. In the present version of the setup, the coupling cannot be tuned once the resonator is assembled. This is not a relevant constraint when the measurements are done at

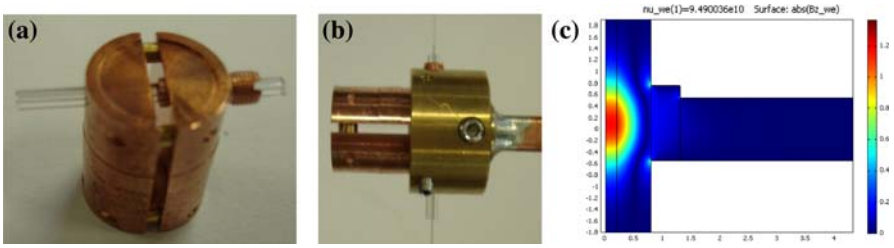

Fig. 2 **a** Assembled view of the NR resonator including the dielectric tube. **b** Assembled resonator with the connection ring and the WR-08 excitation waveguide. **c** Axial magnetic field in half of the axial cross section of the resonator for the TE_{011} mode resonating at 94.9 GHz. On the *right* is the color scale expressed in arbitrary units

room temperature, as for the cases of interest in this work. For the same reasons, no adjustments of the resonance frequency were necessary during the measurements. A control on the coupling level and on the resonance frequency can be implemented as described in Ref. [42].

Figure 2c shows the axial magnetic field distribution of the TE_{011} mode of the NR resonator of Fig. 2a, calculated with the finite-element program Multiphysics 3.5 (Comsol, Sweden) assuming a permittivity $\varepsilon = 3.8$ for Suprasil. In this model, the excitation waveguide is omitted for the sake of simplicity. The resulting structure has cylindrical symmetry and the resulting mode is a pure TE_{011} mode, in which the magnetic field B_{mw} is the strongest on the axis of the resonator. For the same symmetry reasons, the axis of the system is a nodal line for the electric field. Therefore, the preferred sample geometry is cylindrical and limited to a narrow region around the axis.

As discussed above, a convenient placement of the rf coil is close to the sample. A thin metallic wire along the axis of the resonator does not disturb the mode symmetry. Its main effect is a small increase in ohmic losses and thus a slightly reduced quality factor. In principle, such a single wire can serve to couple rf magnetic fields in the NR resonator. However, the B_{rf} field lines are circles around the wire and only a part of the sample inserted around the wire would be excited by suitable rf magnetic field components perpendicular to the static field. Moreover, in view of the characterization of aqueous solutions, it is more convenient to reserve the region around the axis to the insertion of the sample, since the dielectric losses of these systems are expected to reduce the quality factor of the cavity more strongly than a good conductor [48]. For this reason, we have implemented the rf coil in the form of a U-shaped single loop around the sample capillary, using 50 μm copper wires. This also facilitates a simple connection to the rf resonant circuit, where the loop acts as a short on a $\lambda/4$ coaxial rf resonator with a typical Q-factor of about 50. Off-axis wires inserted in the active volume of the mw cavity have been previously employed as ENDOR coils in low-field EPR spectrometers [37, 49, 50].

Numerical modeling shows that the single current loop provides a reasonably homogeneous B_{rf} field around the axis of the resonator. A disadvantage of the present configuration is that the nearby metal wires will lead to susceptibility broadening of the NMR resonance lines. For the present purpose, NMR is mainly

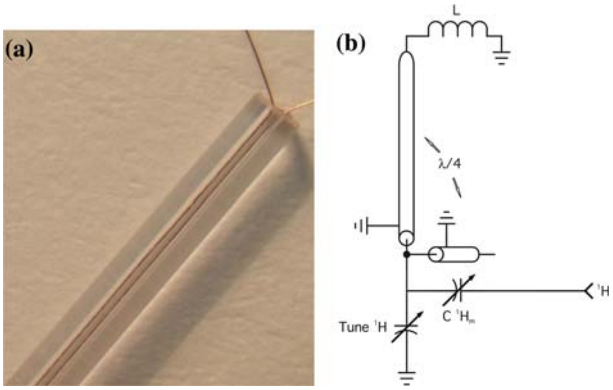

Fig. 3 **a** Picture of the Suprasil tube with the copper wires forming the rf coil. **b** Rf tuning and matching circuit. *L* indicates the single-loop coil inserted in the resonator, *C* is the matching capacitor. The $\lambda/4$ coaxial cable assembly is shown as well

used to monitor the polarization transfer, and therefore, high-resolution spectra are not essential. If needed, the broadening can be reduced by implementation of susceptibility matching fluids in the space between the sample capillary and the dielectric resonator. On the other hand, the wires appear to induce a small displacement of the electric field away from the region internal to the coil. A preliminary analysis confirms that the dielectric absorption of the sample can be reduced, without compromising the magnetic filling factor, by employing a suitable metal shielding. Wind et al. [51] used a helical wire shield around the sample capillary for the same purpose. In principle, such a helix could also be used as a rf microcoil with rf field strengths in the MHz range.

Figure 3a shows a picture of the Suprasil tube with the wires inside. In the final mounting, the wire goes through a Teflon cap at the end of the dielectric tube, as shown in Fig. 1b, c. This cap helps to align the loop in close contact with the inner surface of the dielectric tube. The coil is oriented in order to have the rf field orthogonal to both the mw and the static magnetic field. The structure is quite robust and insensitive to mechanical vibrations. Figure 3b shows the rf tuning and matching circuit, where *L* represents the single-loop coil inserted in the NR resonator.

3 Electromagnetic Characteristics

The mw characteristics of the double-resonance structure were investigated by means of a millimeter-wave vector network analyzer covering the W-band (AB millimetre, France), equipped with a W-band circulator. A typical resonance curve of the device (including the rf coil) is shown in Fig. 4. The resonance curve was normalized to a reference obtained by detuning the resonator. The dashed curve is a Lorentzian fit of the data.

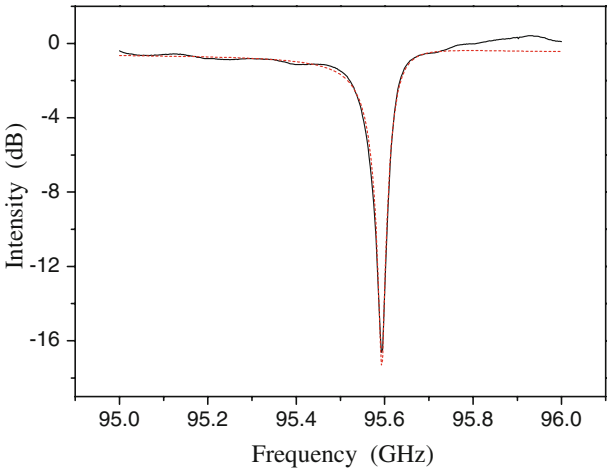

Fig. 4 Resonance curve of the system of Fig. 2, normalized to a reference obtained by detuning the resonator (*solid line*). The *dashed curve* is a Lorentzian fit of the resonance

The loaded quality factor of the resonance is $Q_L = 1300$, which corresponds to the unloaded quality factor $Q_0 = 2100$, according to, e.g., the analysis of Ref. [41]. The quality factor of the mode, together with its field distribution, allows the calculation of the conversion efficiency in any point of the resonator. The conversion efficiency can be expressed in terms of the power-to-magnetic field conversion factor $\bar{B} = \sqrt{\left(\frac{B}{2}\right)^2 \frac{1}{P}}$, where B is the amplitude of the magnetic field and P is the power dissipated in the resonator. The factor 2 takes into account that the circularly polarized component of the magnetic field, which is relevant for magnetic resonances, is half of the linearly polarized field.

For the resonance mode of Fig. 4, the maximum conversion factor along the axis of the resonator is $\bar{B}_{z,\mathrm{mw}} = 1.68\,\mathrm{mT/W^{1/2}}$. The best TE_{011} metallic cavity constructed to date has achieved a $Q_0 = 7400$ at W-band (without any ENDOR option) [52], with a corresponding conversion factor $\bar{B}_{z,\mathrm{mw}} = 1.21\,\mathrm{mT/W^{1/2}}$. Although the quality factor of the double-resonance structure is less than one-third to that of the standard cavity, the conversion factor is considerably higher. This is mainly due to the reduced active volume of the NR dielectric resonator, which rescales with the permittivity approximately as $\varepsilon^{3/2}$. To our knowledge, the obtained conversion factor exceeds any reported value at W-band frequencies.

In the characterization of high-loss materials, the figures of merit of the resonator are strongly affected by the geometry of the sample, with the result that a compromise must be found between the amount of sample and the resulting conversion factor. For the aqueous solutions investigated in this work, an appropriate sample holder is a fused quartz capillary with an outer diameter of 220 μm and an inner diameter of about 60 μm, located concentrically to the dielectric tube. The ends of the capillary were sealed with ultraviolet curable glue. The total sample volume inside the capillary is approximately 40 nl, while the effective volume inside the mw resonator is estimated to be 3 nl.

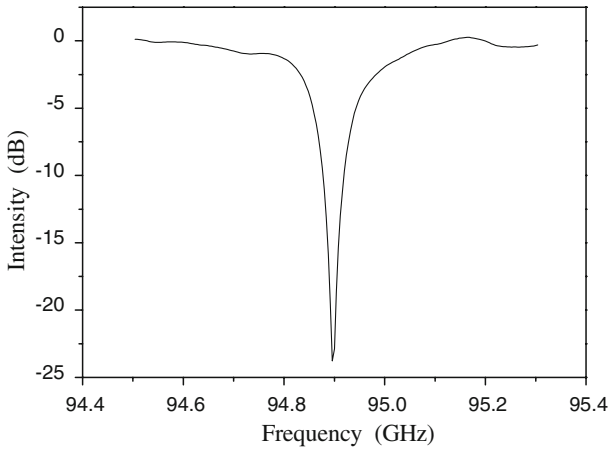

Fig. 5 Resonance curve of the system of Fig. 2 loaded by a 10 mM solution of TEMPO dissolved in a mixture of 40% water and 60% dioxane. The sample holder is a fused quartz capillary with an outer diameter of 220 μm and an inner diameter of 60 μm. The curve is normalized to a reference obtained by detuning the resonator

Figure 5 shows the mw resonance curve obtained by loading the double-resonance structure with a typical aqueous solution employed in this study, in which the TEMPO is dissolved in 40% water and 60% dioxane. The mw quality factor is now $Q_0 = 1600$ and the related conversion factor $\bar{B}_{z,\mathrm{mw}} = 1.51\,\mathrm{mT/W^{1/2}}$. The decrease of the quality factor is partially compensated by the magnetic field increase due to the sample holder [29]. In the typical measurement conditions, the resonator is almost perfectly coupled to the incoming radiation, as shown in Fig. 5.

The rf magnetic field conversion efficiency on the sample was determined from a nutation experiment, where the actual $\pi/2$ pulse length for ^{1}H-NMR measurements was found to be 0.7 μs at power of 100 W. The corresponding conversion factor $\bar{B}_{\mathrm{rf}}$ is 0.8 $\mathrm{mT/W^{1/2}}$ [29]. Bennati et al. [34] used a rf coil placed outside a cylindrical slotted cavity resonating at 140 GHz, leading to a rf conversion factor $\bar{B}_{\mathrm{rf}} = 0.045\,\mathrm{mT/W^{1/2}}$. Weis et al. [28] achieved a rf conversion factor of 0.13 $\mathrm{mT/W^{1/2}}$ by employing a helical mw cavity. More recently, the same design allowed $\bar{B}_{\mathrm{rf}} = 0.17\,\mathrm{mT/W^{1/2}}$ for a system operating at 260 GHz [40]. For the sake of consistency with the mw results, the rf conversion factors have been calculated without normalization to the rf circuit quality factor.

4 DNP Results

As a test for the double-resonance structure, we investigated the polarization transfer from the unpaired electrons of the 4-hydroxy-TEMPO radical to the protons of a mixture of water (40%) and dioxane (60%), in which the radical was dissolved. This mixture was chosen to minimize the dielectric losses of the solvent without affecting the solubility of the radical. TEMPO is probably the most intensively

studied radical in Overhauser DNP experiments, so the DNP performance of the present setup can be compared directly with results from literature. The water–dioxane mixture will have a different DNP performance compared to pure water. For instance, the viscosity is lower, leading to a shorter correlation time and thus a slightly improved Overhauser coupling efficiency at higher magnetic fields. For the present purpose we will ignore such details and concentrate on a characterization of the electromagnetic performance of the probe.

The EPR spectrum of the radical was first characterized by means of continuous-wave (cw) EPR measurements. The spectrometer was composed by a heterodyne W-band bridge delivering a maximum power from 6 to 280 mW, depending on the operation mode. The radiation propagates from the bridge to the resonator through a circulator and a 42 cm long WR-8 single-mode waveguide. The insertion losses of the propagating circuit were estimated at about 3 dB. A modulation coil and an obsolete superconducting Varian NMR magnet with a 45 mm warm bore completed the spectrometer. A small sweep coil was incorporated in the double-resonance probe to allow field-swept measurements.

Figure 6 shows the EPR spectra of several samples differing in radical concentration. The spectra are obtained by modulating the static field at 100 Hz, with an amplitude of 0.15 mT. The mw power at the resonator for the cw EPR measurements was about 50 μW. The lock-in integration constant was set at 0.3 s. The estimated sensitivity for these measurements is 10^{11} spins/mT.

The characteristic hyperfine spectrum of the unpaired $S = \frac{1}{2}$ electron spin interacting with the $I = 1$ nuclear spin of ^{14}N is in good agreement with literature and simulated data. At higher concentrations, the exchange coupling between the unpaired electrons increases the line width of the EPR resonances.

The ^{1}H-NMR spectrum of the sample was obtained by means of the usual pulsed technique, consisting in the analysis of the free induction decay after a $\frac{\pi}{2}$ pulse. The NMR spectrometer in this case was a homebuilt instrument *based* on a PC-*based*

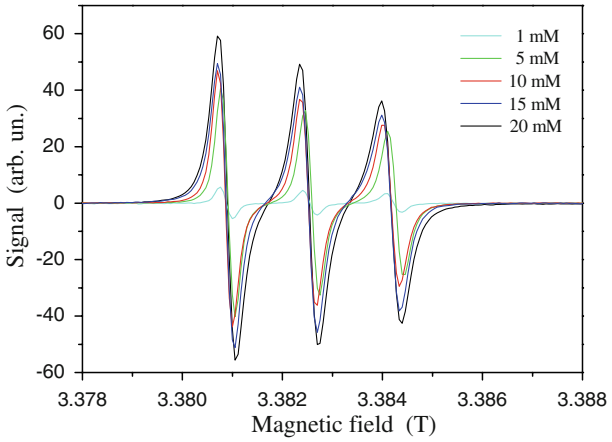

Fig. 6 CW EPR spectra of TEMPO, dissolved in 40% water and 60% dioxane, at different concentrations. Larger EPR lines correspond to higher concentrations. The power at the resonator in these measurements was 50 μW

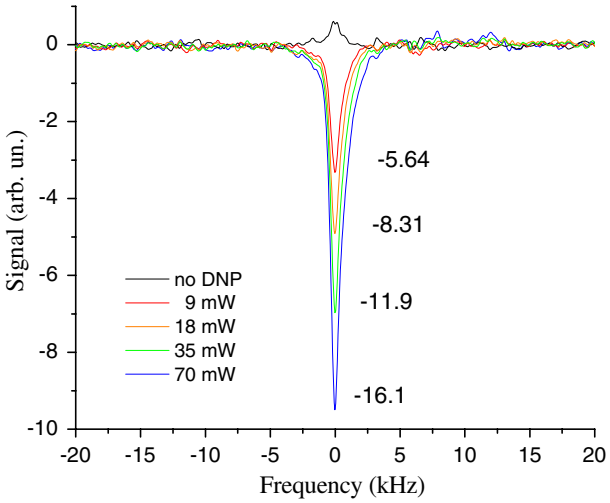

Fig. 7 ^{1}H-NMR spectra of the 10 mM solution of TEMPO in 40% water and 60% dioxane for various mw powers. *The curve with the positive peak* refers to the case without mW. The *negative peak* generated by the mW irradiation increases with the power; the related enhancement is reported *on the right of the curves*. The maximum power delivered by the source in these measurements was 140 mW

pulse programmer (Spincore PulseBlaster), National Instruments data acquisition cards and Matlab-based software. Figure 7 shows the NMR spectra obtained for the 10 mM solution of TEMPO, with and without mw irradiation. Four scans were averaged to allow a full phase cycle. A rather substantial broad proton background signal was subtracted by taking a reference for an empty sample capillary. In the present setup, the NMR resolution is limited due to field distortions by the probe, the sweep coil, and imperfections in the NMR magnet itself. For this reason, we do not resolve the separate water and dioxane resonances.

The DNP signal enhancement is obtained under variable power cw pumping on the second line of the EPR triplet. The effect of the mw irradiation is to invert and eventually enhance the NMR signal. This behavior is typical for Overhauser DNP with dipolar coupling between electron and nuclear spins, which is indeed the dominant coupling for the nitroxide radical in aqueous solutions [53]. A maximum enhancement of -16 has been obtained.

The progression of the DNP enhancement with the mw power is reported in Fig. 8 for different samples. It turned out that 10 mM is the radical concentration allowing the highest enhancement. A quantitative analysis of the obtained results requires the determination of the polarization transfer parameters, which is beyond the scope of this paper. The solid lines are fits using the classical expressions for Overhauser dipolar coupling [51, 53].

It is worthwhile to note that in the present case it is not straightforward to give an absolute number for the enhancement. On one hand, the NMR signal is measured for the full capillary length (40 nl of sample), while only the part of the capillary corresponding to the mw resonator is subject to mw irradiation, thus leading to an

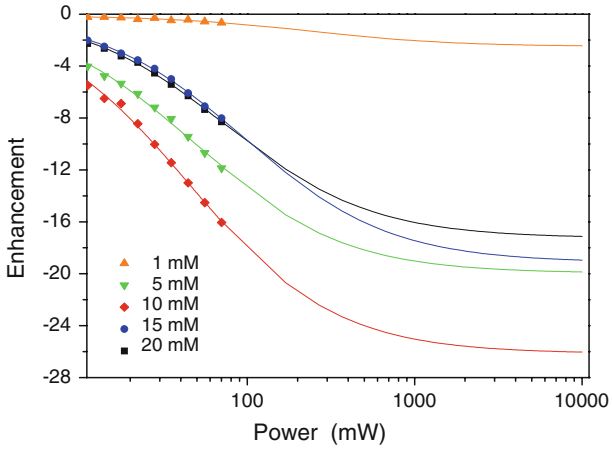

Fig. 8 Experimental dependence of the DNP enhancement of the TEMPO solution in 40% water and 60% dioxane as a function of the mw power (*points*) for the various investigated concentrations. The *solid lines* are the fits of the experimental points (see the text)

inverted DNP signal (3 nl of sample). This would suggest that the actual enhancement is much bigger. On the other hand, due to field gradients, the NMR signal from the outer ends of the capillary is spread over a larger spectral region and the normalization procedure is not exact. For this reason, we have used the enhancement observed at the peak position, which is a conservative lower estimate of the actual DNP effect. Additional measurements aimed at an improved NMR resolution are underway to resolve this issue.

A problem often affecting the DNP measurements on high dielectric loss materials is given by the heating of the sample. As anticipated, the use of a resonant structure can mitigate this problem, although a residual dielectric absorption is necessarily present. The fraction of mw energy dissipated in the sample can be determined by considering the variation of the quality factor of the resonant structure due to the insertion of the sample. In our case, such variation indicates that about 24% of the power coupled to the resonator is dissipated in the system formed by the sample and the sample holder. This corresponds to about 17 mW for the measurements at the highest available power. According to the analysis of Ref. [54], a sample heating by a few degrees centigrade is expected. This heating will induce a shift of the NMR line less than a ppm. Within the experimental accuracy, we see no shift of the resonance line, which confirms the limited sample heating.

5 Conclusions

The main difficulties encountered so far in the design of a DNP double-resonance structure with very high conversion factor in both its mw and rf responses can be overcome by combining an open NR resonator with an intracavity rf coil, as demonstrated by the obtained results.

The state-of-the-art conversion factor demonstrated at 95 GHz, 1.68 mT/W$^{1/2}$, can be compared with the value estimated for the free space propagation of a linearly polarized wave, 0.02 mT/W$^{1/2}$, obtained under the assumption of an ideal focalization of the mw beam over a surface of λ_0^2. These values show that, without resonant structure, 10^4 more mw power can be required to reach the same level of saturation for the EPR transitions. At the same time, the use of the proposed resonant structure allows a careful control of the heating of the sample due to its dielectric absorption. As such the presented design can also be of great relevance for standard EPR and ENDOR techniques.

At the basis of the performance of the proposed double-resonance system there is a single-mode dielectric resonator, characterized by small active volume, simple structure, and large axial access. The small area of the rf coil is the other key aspect of the system, in which the coil is axially inserted in the form of a single-loop 'hairpin' coil. With this geometry, the presence of the rf coil induces only a limited reduction of the quality factor of the mw resonator. Moreover, no special care is required for the isolation of the coil, which is already surrounded by dielectric regions. The overall structure appears robust and unaffected by vibration problems. It can be further improved by integrating the rf coil directly on the dielectric sample holder, for instance, by means of a metal coating.

The proposed design can be employed at higher frequencies, where the main obstacle is represented by the very small size of the resonator. Previous results show that this approach is viable at least up to 300 GHz [41]. At higher frequencies, a possible solution is to employ quasi-single-mode NR structures. In conclusion, the integration of miniaturized rf coils inside open NR resonators seems capable to establish a new perspective in the development of instrumentation for high-field magnetic resonances.

Acknowledgments We kindly acknowledge Nederlandse Organisatie voor Wetenschappelijk Onderzoek (NWO), the European Cooperation in Science and Technology (COST) action P15 "Advanced paramagnetic resonance methods in molecular biophysics", and the Short-Term Mobility programme of the National Research Council (CNR) for the financial support.

References

1. A.W. Overhauser, Phys. Rev. **92**, 411 (1953)
2. T.R. Carver, C.P. Slichter, Phys. Rev. **92**, 212 (1953)
3. A. Abragam, *The Principles of Nuclear Magnetism* (Clarendon, Oxford, 1961)
4. A.V. Kessenikh, V.I. Lushchikov, A.A. Manenkov, Y.V. Taran, Sov. Phys. Solid State **5**, 321 (1963)
5. A.V. Kessenikh, A.A. Manenkov, G.I. Pyatnitskii, Sov. Phys. Solid State **6**, 641 (1964)
6. C.F. Hwang, D.A. Hill, Phys. Rev. Lett. **18**, 110 (1967)
7. C.F. Hwang, D.A. Hill, Phys. Rev. Lett. **19**, 1011 (1967)
8. D.S. Wollan, Phys. Rev. B **13**, 3671 (1976)
9. R.A. Wind, M.J. Duijvestijn, C. van der Luat, A. Manenschijn, J. Vriend, Prog. Nucl. Magn. Reson. Spectrosc. **17**, 33 (1985)
10. T. Maly, G.T. Debelouchina, V.S. Bajaj, K.N. Hu, C.G. Joo, M.L. Mak-Jurkauskas, J.R. Sirigiri, P.C.A. van der Wel, J. Herzfeld, R.J. Temkin, R.G. Griffin, J. Chem. Phys. **128**, 052211 (2008)
11. K.H. Hausser, D. Stehlik, Adv. Magn. Reson. **3**, 79 (1968)
12. G. Denninger, W. Stocklein, E. Dormann, M. Schwoerer, Mol. Cryst. Liq. Cryst. **120**, 233–236 (1985)

13. K.N. Hu, H.H. Yu, T.M. Swager, R.G. Griffin, J. Am. Chem. Soc. **126**, 10844–10845 (2004)
14. C. Song, K.N. Hu, C.G. Joo, T.M. Swager, R.G. Griffin, J. Am. Chem. Soc. **128**, 11385–11390 (2006)
15. E.R. McCarney, B.D. Armstrong, M.D. Lingwood, S. Han, Proc. Natl. Acad. Sci. USA **104**, 1754–1759 (2007)
16. B.D. Armstrong, S. Han, J. Am. Chem. Soc. **131**, 4641–4647 (2009)
17. J.H. Ardenkjaer-Larsen, B. Fridlund, A. Gram, G. Hansson, L. Hansson, M.H. Lerche, R. Servin, M. Thaning, K. Golman, Proc. Natl. Acad. Sci. USA **100**, 10158–10163 (2003)
18. Appl. Magn. Reson. **34** (2008)
19. L. Frydman, C. R. Chim. **9**, 336–345 (2006)
20. Y. Shrot, L. Frydman, J. Magn. Reson. **195**, 226–231 (2008)
21. Y. Shrot, L. Frydman, J. Chem. Phys. **128**, 052209 (2008)
22. Y. Shrot, L. Frydman, J. Chem. Phys. **128**, 164513 (2008)
23. L.R. Becerra, G.J. Gerfen, R.J. Temkin, D.J. Singel, R.G. Griffin, Phys. Rev. Lett. **71**, 3561 (1993)
24. M.K. Hornstein, V.S. Bajaj, R.G. Griffin, K.E. Kreischer, I. Mastovsky, M.A. Shapiro, J.R. Sirigiri, IEEE Trans. Electron Devices **52**, 798–807 (2005)
25. V.S. Bajaj, M.K. Hornstein, K.E. Kreischer, J.R. Sirigiri, P.P. Woskov, M.L. Mak-Jurkauskas, J. Herzfeld, R.J. Temkin, R.G. Griffin, J. Magn. Reson. **189**, 251–279 (2007)
26. T. Idehara, T. Saito, I. Ogawa, S. Mitsudo, Y. Tatematsu, L. Agusu, H. Mori, S. Kobayashi, Appl. Magn. Reson. **34**, 265–275 (2008)
27. M. Glyavin, V. Khizhnyak, A. Luchinin, T. Idehara, T. Saito, Int. J. Infrared Millimeter Waves **29**, 641–648 (2008)
28. V. Weis, M. Bennati, M. Rosay, J.A. Bryant, R.G. Griffin, J. Magn. Reson. **140**, 293–299 (1999)
29. C.P. Poole, *Electron Spin Resonance: a Comprehensive Treatise on Experimental Techniques* (Wiley, New York, 1983)
30. A.P.M. Kentgens, J. Bart, P.J.M. van Bentum, A. Brinkmann, E.R.H. Van Eck, J.G.E. Gardeniers, J.W.G. Janssen, P. Knijn, S. Vasa, M.H.W. Verkuijlen, J. Chem. Phys. **128**, 052202 (2008)
31. D.J. Singel, H. Seidel, R.D. Kendrick, C.S. Yannoni, J. Magn. Reson. **81**, 145–161 (1989)
32. R.A. Wind, R.A. Hall, A. Jurkiewicz, H. Lock, G.E. Maciel, J. Magn. Reson. **A110**, 33–37 (1994)
33. H. Cho, J. Baugh, C.A. Ryan, D.G. Cory, C. Ramanathan, J. Magn. Reson. **187**, 242–250 (2007)
34. M. Bennati, C.T. Farrar, J.A. Bryant, S.J. Inati, V. Weis, G.J. Gerfen, P. Riggs-Gelasco, J. Stubbe, R.G. Griffin, J. Magn. Reson. **138**, 232–243 (1999)
35. P. Hofer, G. Parigi, C. Luchinat, P. Carl, G. Guthausen, M. Reese, T. Carlomagno, C. Griesinger, M. Bennati, J. Am. Chem. Soc. **130**, 3254 (2008)
36. J.S. Hyde, J. Chem. Phys. **43**, 1806 (1965)
37. K.P. Dinse, K. Möbius, R. Biehl, Z. Naturforsch. **28a**, 1069 (1973)
38. I.M. Brown, D.J. Sloop, Rev. Sci. Instrum. **41**, 1774 (1970)
39. K. Gruber, J. Forrer, A. Schweiger, H.H. Gunthard, J. Phys. E Sci. Istrum. **7**, 569–576 (1973)
40. V.P. Denysenkov, M.J. Prandolini, A. Krahn, M. Gafurov, B. Endeward, T.F. Prisner, Appl. Magn. Reson. **34**, 289–299 (2008)
41. G. Annino, M. Cassettari, M. Martinelli, IEEE Trans. Microwave Theory Tech. **57**, 775–783 (2009)
42. G. Annino, M. Fittipaldi, M. Martinelli, H. Moons, S. Van Doorslaer, E Goovaerts. J. Magn. Reson. **200**, 29–37 (2009). doi:10.1016/j.jmr.2009.05.011
43. G. Annino, M. Cassettari, M. Martinelli, P.J.M. van Bentum, Appl. Magn. Reson. **24**, 157–175 (2003)
44. G. Annino, M. Cassettari, M. Fittipaldi, M. Martinelli, J. Magn. Reson. **176**, 37–46 (2005)
45. G. Annino, M. Cassettari, M. Martinelli, Rev. Sci. Instrum. **76**, 084702 (2005)
46. G. Annino, M. Cassettari, M. Martinelli, Rev. Sci. Instrum. **76**, 064702 (2005)
47. G. Annino, M. Cassettari, M. Martinelli, Appl. Magn. Reson. **26**, 447–456 (2004)
48. J. Krupka, A. Milewski, J. Phys. E Sci. Instrum. **12**, 391–396 (1979)
49. H. Seidel, Z. Phys. **165**, 239 (1961)
50. I. Tkach, A. Baldansuren, E. Kalabukhova, S. Lukin, A. Sitnikov, A. Tsvir, M. Ischenko, Y. Rosentzweig, E. Roduner, Appl. Magn. Reson. **35**, 95–112 (2008)
51. R.A. Wind, J.H. Ardenkjaer-Larsen, J. Magn. Reson. **141**, 347–354 (1999)
52. A. Savitsky, A.A. Dubinskii, M. Plato, Y.A. Grishin, H. Zimmermann, K. Möbius, J. Phys. Chem. B **112**, 9079–9090 (2008)
53. B.D. Armstrong, S. Han, J. Chem. Phys. **127**, 104508 (2007)
54. M.J. Prandolini, V.P. Denysenkov, M. Gafurov, S. Lyubenova, B. Endeward, M. Bennati, T.F. Prisner, Appl. Magn. Reson. **34**, 399–407 (2008)